

North-South non-Gaussian asymmetry in Planck CMB maps

A. Bernui^a A. F. Oliveira^b T. S. Pereira^c

^aObservatório Nacional, Rua General José Cristino 77, São Cristóvão, 20921-400 Rio de Janeiro – RJ, Brazil

^bInstituto de Física e Química, Universidade Federal de Itajubá, 37500-903 Itajubá – MG, Brazil

^cDepartamento de Física, Universidade Estadual de Londrina, Rod. Celso Garcia Cid, Km 380, 86057-970, Londrina – PR, Brazil

E-mail: abernui@gmail.com, adhimar@unifei.edu.br, tspereira@uel.br

Abstract. We report the results of a statistical analysis performed with the four foreground-cleaned Planck maps by means of a suitably defined *local-variance* estimator. Our analysis shows a clear dipolar structure in Planck’s *variance map* pointing in the direction $(l, b) \simeq (220^\circ, -32^\circ)$, thus consistent with the North-South asymmetry phenomenon. Surprisingly, and contrary to previous findings, removing the CMB quadrupole and octopole makes the asymmetry stronger. Our results show a maximal statistical significance, of 98.1% CL, in the scales ranging from $\ell = 4$ to $\ell = 500$. Additionally, through exhaustive analyses of the four foreground-cleaned and individual frequency Planck maps, we find unlikely that residual foregrounds could be causing this dipole variance asymmetry. Moreover, we find that the dipole gets lower amplitudes for larger masks, evidencing that most of the contribution to the variance dipole comes from a region near the galactic plane. Finally, our results are robust against different foreground cleaning procedures, different Planck masks, pixelization parameters, and the addition of inhomogeneous real noise.

Contents

1	Introduction	1
2	Foreground-reduced Planck maps	2
3	The variance estimator	3
3.1	Statistically Isotropic Gaussian maps	4
4	Statistical estimator applied to Planck maps	5
4.1	Angular power spectra analyses of V -maps	5
4.2	Angular-scale analyses of the Variance dipole	8
4.3	Masks and foreground residuals effects on Variance dipole	9
5	Concluding remarks	11
	References	13

1 Introduction

The temperature fluctuations of the Cosmic Microwave Background radiation (CMB), recently released by the *Planck collaboration* [1], confirmed with outstanding precision the concordance cosmological model, Λ CDM [2–4]. Such exquisite set of cosmological information allows us to test two fundamental properties of the universe expected after the standard inflationary phase [5–8], namely that the CMB field is, at large-angles, nearly Gaussian and statistically isotropic (see, e.g., [9, 10] and refs. therein).

Previous studies using WMAP data indicate significant departure from either gaussianity or statistical isotropy at the largest angular scales – an unexpected result in the Λ CDM model [11–57], though possibly disputable [58]. These phenomena, also called *anomalies*, have been now confirmed with similar high confidence levels, $\sim 3\sigma$, by the *Planck collaboration* with CMB foreground-cleaned maps [10]. On the other side, only small magnitude Gaussian deviations from primordial origin have been detected in Planck data [59, 60]. However, there are more potential sources of non-Gaussianity (NG) in the CMB data than just primordial NG [61–66]. These include galactic foregrounds remnants and secondary anisotropies coming from processes after the last scattering surface [60, 67–82]. In particular, Gaussian analyses for large angular scales are delicate because galactic foregrounds contaminations are not completely understood and, as a consequence, galactic cut-sky masks are still necessary in CMB data analyses [60]. Monteserín et al. (2008) [83] reported an anomalously low variance distribution in WMAP3 maps at 98.7% CL. Cruz et al. (2011)[84] confirmed this result in WMAP5 and WMAP7 data, also pointing that some regions near the galactic plane present an anomalously high variance (95.6% CL) in the south ecliptic hemisphere. Their analyses, using various galactic cut-sky masks, suggest that foreground residuals could explain the results, besides a possible connection with the CMB quadrupole-octopole alignment was investigated. Gruppuso et al. (2013) [?], using a different estimator, also found a low variance at large scales in WMAP9 data, basically in agreement with [83, 84]. More recently, the *Planck collaboration* [10] and Akrami et al. (2014) [85] studied the local variance in hemispheres and disks finding again an anomalous high variance in the south ecliptic hemisphere.

In recent works [86–88] one of us have proposed two large-angle NG estimators based on skewness and kurtosis momenta performed on spherical caps on the CMB sphere. We found that this directional mapping approach is suitable when a cut-sky mask has to be used because it minimizes the effect of incomplete data in the CMB sky. These indicators provide a directional map of local NG due to its possible non-uniform distribution in the CMB maps, also giving information about the angular scale dependence of such contributions. Results obtained in previous analyses [86, 87] using WMAP maps suggest that the NG captured there is not of primordial origin, although it might have a primordial component.

The aim of the present work is to conduct an analysis of the local variance in Planck foreground-cleaned maps, using a prescription similar to that of Refs. [86–88]. For this we implement a simple estimator of statistical variance, applying it to patches of the CMB sky. The information from all the patches is then used to produce an associated *Variance*-map, or simply *V*-map, which contains the signatures of the analysed CMB map. Our analyses investigate the possibility that foreground remnants in the galactic region could be the source of departures from Gaussianity and statistical isotropy, by considering several cut-sky Planck masks and three frequency band Planck maps, in addition to the four foreground-cleaned maps. To calculate the confidence level of our results we shall compare properties of these *V*-maps from Planck data with *V*-maps from simulated Monte Carlo (MC) CMB maps. These maps are obtained as Gaussian and statistically isotropic realisations from a seed angular power spectrum corresponding to the Λ CDM concordance model. Accordingly, the masking procedure applied to Planck CMB data is also applied to the MC maps.

In section 2 we briefly review the main features of the four foreground-cleaned *Planck* maps and the masks to be used in the analyses. In section 3 we describe our variance estimator and explain the methodology to study the statistical Gaussian and isotropy attributes of Planck maps. The procedure delineated in this section will be used, in section 4, to investigate directional large-angle deviations from the standard statistical scenario of the Planck data as compared with simulated maps. Our analysis includes realistic features of the Planck data, like their inhomogeneous noise maps and galactic cut-sky masks. Finally, in section 5, we summarize our main results, present our conclusions and final remarks.

2 Foreground-reduced Planck maps

The Planck satellite observed the sky in nine frequency bands, from 30 to 857 GHz [1, 89]. The use of four *component separation techniques*, which efficiently identifies the sources of contaminating emissions present in the data set, have allowed the *Planck collaboration* to produce four high resolution and almost full sky foreground-cleaned CMB maps [89]. They are: the Spectral Matching Independent Component Analysis (SMICA) [90], the Needlet Internal Linear Combination (NILC) [73], the Internal Template Fitting Spectral Estimation Via Expectation Maximization (SEVEM) [91], and the combined approach termed Commander-Ruler (CR) [89, 92].

Each of the foreground cleaning methods provides a CMB map with its Component Separation Confidence mask –also termed *validation* mask or simply VALmask– outside which the corresponding CMB data is considered to be foreground-cleaned, and also a noise map containing an estimate of the real inhomogeneous pixel’s noise. In addition, the SMICA and NILC maps were released with their own *inpainting* mask, or simply INPmask. Regarding the masks, there also exist the separation component minimum mask, termed M82, and the U73

mask, which is the union of the confidence galactic masks plus the point sources mask [89] (see Table 1).

The effect of realistic anisotropic noise, due to the different number of times that each pixel was observed by the probe, is taken into account according to the specifications of each foreground-cleaned method. For this, each component separation procedure provides an estimate of the pixel’s noise in the output CMB map, information released together with each foreground-cleaned Planck map as a full-sky map, termed *noise map* [10, 60, 89]. Thus, we use the noise maps in a “signal + noise” analysis to find their effect on *V*–maps, i.e., we apply our estimator after adding a noise map to its corresponding foreground-cleaned Planck map. In section 4 we consider the analyses with and without including this realistic anisotropic noise component, which is done by adding to the foreground-cleaned map its corresponding noise map, and also considering different Planck masks.

Planck mask	f_{sky}
SMICA – INPMASK	0.97
SMICA – VALMASK	0.89
NILC – INPMASK	0.97
NILC – VALMASK	0.93
SEVEM – VALMASK	0.76
CR – VALMASK	0.75
M82 – MINIMAL MASK	0.82
U73 – UNION MASK	0.73

Table 1. The f_{sky} values give the available sky fraction of a CMB map when a Planck mask is applied to it.

3 The variance estimator

We start this section by explaining the procedure for constructing the variance map (*V*–map) of a given CMB map. Let $\Omega_j \equiv \Omega(\theta_j, \phi_j) \in \mathbb{S}^2$ be a hemisphere on the celestial sphere, with center at the j^{th} pixel, $j = 1, \dots, N_{\text{hem}}$, where (θ_j, ϕ_j) are the angular coordinates of the j^{th} pixel, and N_{hem} is the number of hemispheres. The number of hemispheres and the coordinates of their centers are defined using the HEALPix pixelization scheme [93]. Moreover, the hemisphere’s centers are uniformly distributed on \mathbb{S}^2 and the union of them completely covers the celestial sphere.

The variance of the data inside each hemisphere can be calculated simply by

$$V_j = \frac{1}{n_p} \sum_{i=1}^{n_p} (T_j^i - \overline{T_j})^2, \quad (3.1)$$

where n_p is the number of pixels in the j^{th} hemisphere, T_j^i is the temperature fluctuation at the i^{th} pixel and $\overline{T_j}$ is the mean CMB temperature fluctuation of the j^{th} hemisphere.

The values V_j obtained in this way give a local measure of the variance in the direction (θ_j, ϕ_j) . Patching together the set of values $\{V_j, j = 1, \dots, N_{\text{hem}}\}$ in a sphere with N_{hem} pixels we obtain a colored (pixelized) celestial sphere. The Mollweide projection of this sphere is termed the *V*–map: it is the final product of the application of our variance estimator to a

given CMB map. According to the scale of colors, the minimum (maximum) value of the set $\{V_j\}$ corresponds to the bluest (reddest) pixel. With the above prescription one can obtain a quantitative measure of anomaly of a real map by simply calculating the angular power spectrum of its corresponding V -map, and then comparing it with the mean power spectra obtained from MC simulations.

Because the V -map assigns a real value to each pixel in the celestial sphere \mathbb{S}^2 , that is $V = V(\theta, \phi)$, one can expand it in spherical harmonics: $V(\theta, \phi) = \sum_{L,M} A_{LM} Y_{LM}(\theta, \phi)$, where the set of values $\{v_L, L = 0, 1, 2, \dots\}$, given by

$$v_L \equiv \frac{1}{2L+1} \sum_{M=-L}^L |A_{LM}|^2, \quad (3.2)$$

is the angular power spectrum of the V -map. Given that we are interested in the large-scale NG deviations, we shall concentrate on the low- L angular power spectrum $\{v_L, \text{for } L = 1, 2, \dots, 10\}$ of the V -map.

Before proceeding, let us clarify some points of our whole prescription. In what concerns the implementation of a local variance estimator, note that Eq. (3.1) is the simplest mathematical possibility. On the other hand, the choice of spherical caps with an aperture of 90° is motivated by the fact that, when scanning a map to calculate its V -map, the procedure considers caps whose centers are close or even within the masked region. In these cases, the variance of the data inside the cap is performed with a smaller number of pixels, which introduces additional statistical noise as compared to caps away from the masked region. As it turns out, this effect can be minimized by choosing spherical caps having aperture of 90° , that is, hemispheres [86–88]. Note that our prescription is thus different from the one adopted in [85], where not only the size of the caps is allowed to vary, but also masked pixels are excluded. As we will see, our results are compatible with their findings.

In the next section we use the above procedure to generate V -maps from the set of 1,000 Gaussian and statistically isotropic simulated maps – from now on called V^G -maps – from which we obtain the corresponding spectra, v_L^G , and mean values, \bar{v}_L^G . We then compare the spectra of the V -maps produced from the Planck maps, from now on called V^{PLA} -maps, with the mean value \bar{v}_L^G . We finally emphasize that, although it might be clear from the context, the V^G -maps themselves are not normally distributed.

3.1 Statistically Isotropic Gaussian maps

Our Gaussian and statistically isotropic MC maps were obtained as random realizations from a seed angular power spectrum, which corresponds to the Λ CDM concordance model [1], and the map-making process is performed using the SYNFAST facility from the HEALPix package [93]. We test the robustness of our outcomes with two different angular resolutions of the V -maps, that is, with $N_{\text{hem}} = 768$ and with $N_{\text{hem}} = 3,072$. For illustration, we show in Fig. 1 two representative V^G -maps from a MC simulations; notice in these figures the minimum and the maximum values.

In order to generate a V -map, either from a MC or foreground-cleaned Planck map, we first choose the angular scales to be included in analysis, $\ell \in [\ell_{\text{min}}, \ell_{\text{max}}]$, which in turn determine the angular resolution (N_{side}) of the map. Planck and simulated CMB maps are analysed under the same conditions: mask, angular-scale’s interval, N_{side} , and N_{hem} . Thus, given the set of 1,000 MC maps, we produce their corresponding 1,000 V^G -maps and calculate their associated power spectra, namely, $\{\{v_L\}^{\mathbf{i}}\}$, for $\mathbf{i} = 1, \dots, 1,000$ and $L = 1, \dots, 10$.

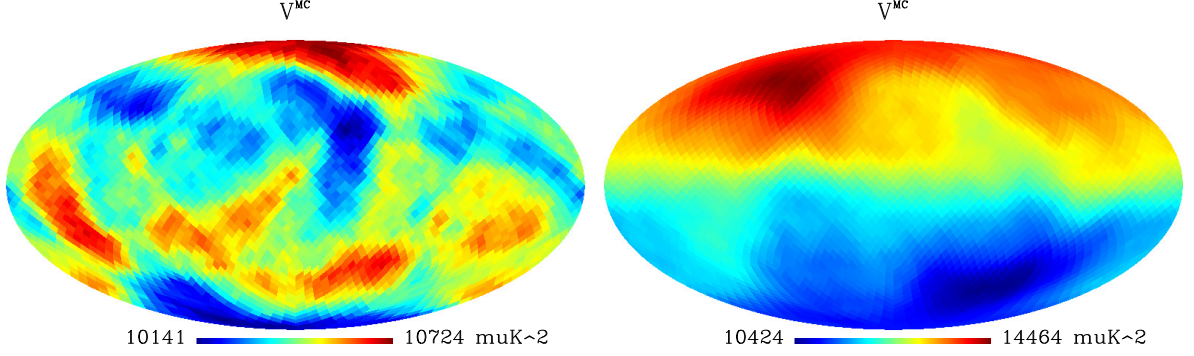


Figure 1. Variance maps from Gaussian and statistically isotropic simulations. We show V^G -maps with the minimum (left, smaller than the data) and the maximum (right, larger than the data) variance dipole values produced from the set of 1,000 MC CMB maps, in units of μK^2 .

Finally, we compute the mean angular power spectra of the V^G -maps

$$\bar{v}_L^G = \frac{1}{1000} \sum_{i=1}^{1000} v_L^i. \quad (3.3)$$

These values are then used to obtain the statistical significance (i.e., the goodness-of-fit) of the spectrum v_L^{PLA} , obtained from the V^{PLA} -map.

4 Statistical estimator applied to Planck maps

In this section we perform variance analyses of the four foreground-cleaned Planck maps. We first calculate their angular power spectra v_L^{PLA} , and the corresponding statistical confidence level by comparison with the mean spectra \bar{v}_L^G . We find that the dipolar term of the v_L^{PLA} 's spectra is the dominant term, and appears to be robust under foreground-cleaning procedures (i.e., a similar result is obtained for the four Planck maps), cut-sky masks, inhomogeneous pixel's noise, and different estimator's parameter N_{hem} . Then we investigate several angular scale's intervals looking for the origin of this variance dipole phenomenon. At the end of this section we discuss the possibility that residual foregrounds could be causing it.

4.1 Angular power spectra analyses of V -maps

The CMB maps analysed in this subsection contain the angular-scales $\ell \in [2, 1,000]$. We shall study two cases: the 'pure signal' case and the 'signal + inhomogeneous noise' case. Initially we use $N_{\text{side}} = 512$, $N_{\text{hem}} = 3,072$, but to validate our results of this subsection we also consider other pixelization scheme's parameters as robustness tests.

The result of the application of our estimator on the four foreground-cleaned Planck maps can be observed in Fig. 2, where we show the V^{PLA} -maps obtained using the four Planck maps and diverse masks. A common interesting feature noticed in these V -maps is the strong dipolar signal, independent of the maps and masks used to produce the V^{PLA} -map. Similar results are obtained in all the other cases investigated, which we do not show in Fig. 2 to avoid repetitions.

In Fig. 3 we give a quantitative measure of the spectra of the V^{PLA} -maps as compared with the average spectra of the V^G -maps (for simplicity we present only the SMICA + VALmask case; the other cases show similar results). This comparison measures the possible

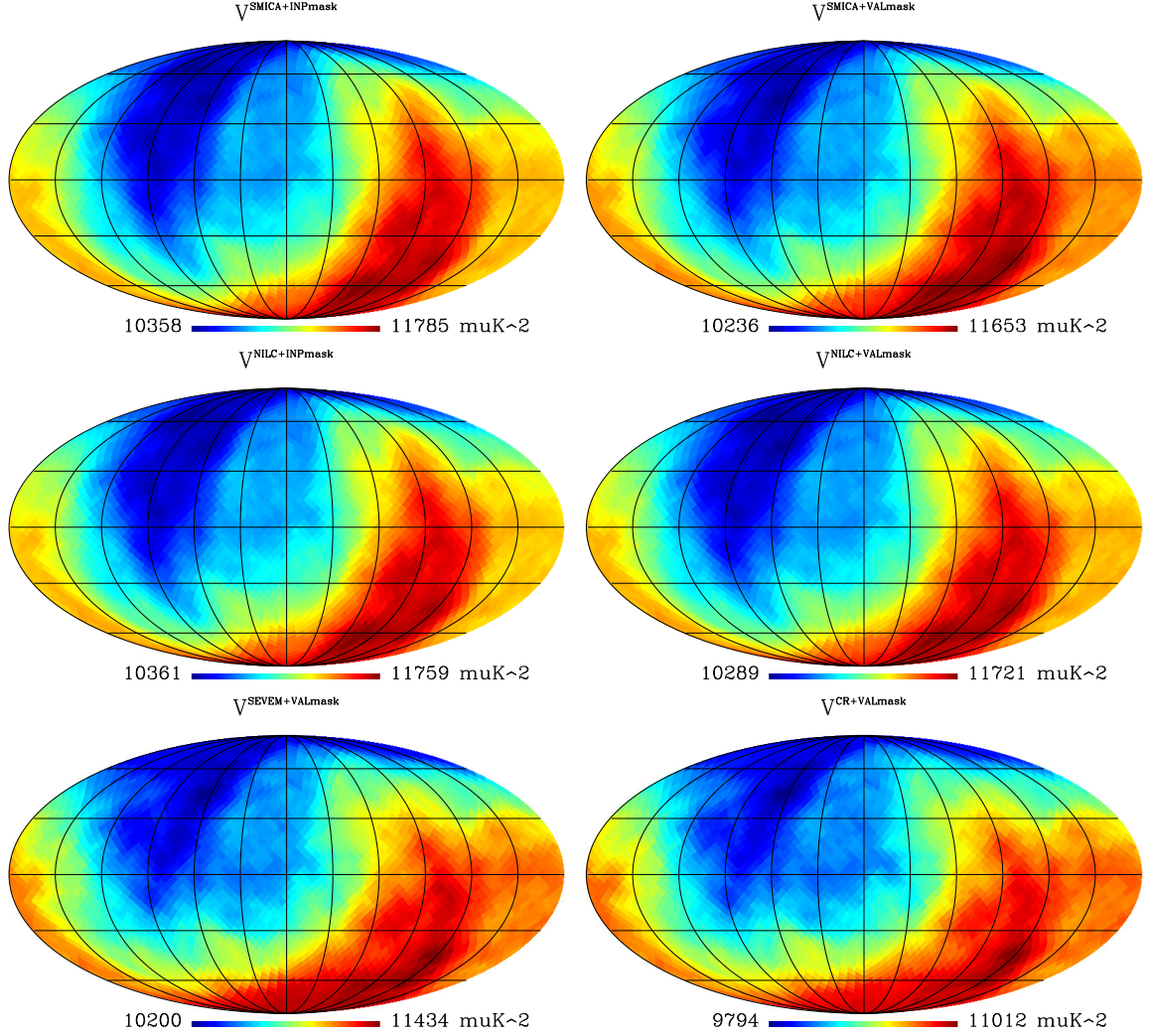


Figure 2. Variance maps of four different foreground-cleaned Planck maps. In the top row we have the V -maps obtained from the foreground-cleaned SMICA Planck map using their INPmask (left) and VALmask (right). Similarly, in the middle row we show the V -maps obtained from the foreground-cleaned NILC Planck map using their INPmask (left) and VALmask (right), respectively. Finally, in the bottom row we have the V -maps obtained from the foreground-cleaned SEVEM (left) and CR (right) Planck maps using their corresponding VALmasks.

departure of the Planck data with respect to the standard statistical scenario. In fact, an overall assessment of the statistical significance of the spectrum v_L^{PLA} as compared with the average spectra \bar{v}_L^{G} data, given by the χ^2 goodness-of-fit, supplies a measure of the statistical features present in Planck data. For instance, in Fig. 3 the goodness-of-fit test gives $\chi^2 = 7.3$, for 9 d.o.f. (degrees of freedom), which means a good agreement between Planck data and Gaussian MCs, having in mind the large cosmic variance existent at these scales. Similar numerical analyses can be obtained for other cases.

As suggested by the Planck team [60], realistic experimental features such as galactic masks and anisotropic noise distribution should be used in Planck data analyses to test the robustness of the results. Moreover, because these noise maps have a large quadrupolar

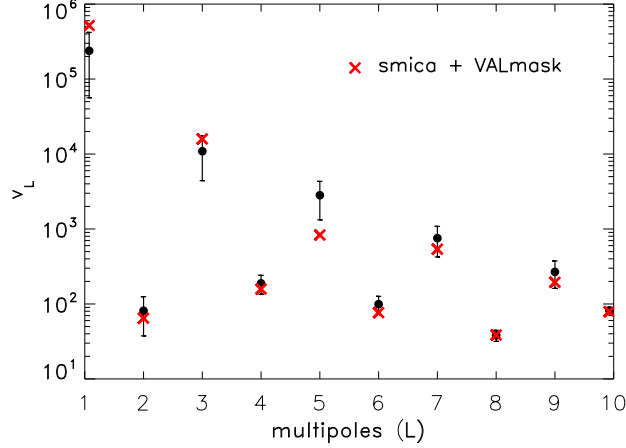


Figure 3. Angular power spectrum of the V^{SMICA} -map, generated applying our estimator to the SMICA Planck map, after cutting the sky patch corresponding to its VALmask. The average spectrum \bar{v}_L^G generated from Gaussian and statistically isotropic CMB data is represented as dots with 1σ error bars. The χ^2 goodness-of-fit gives 7.3, for 9 d.o.f., corresponds to a p -value equal to 0.61, which lead us to conclude that this spectrum is fully consistent with the null hypothesis (i.e., a Gaussian and statistically isotropic universe). The V^{SMICA} -map for this case, i.e., SMICA map + VALmask, is seen in the right panel of the first row in Fig. 2, where the dipole variance points towards $(l, b) \simeq (245^\circ, -35^\circ)$.

signal roughly aligned with the ecliptic, it is pertinent to evaluate the effect of such real anisotropic noise by comparing the cases with and without noise. For this, we calculate the χ^2 values, for 9 d.o.f., considering the four foreground-cleaned Planck maps in different situations: considering the addition or not of their corresponding anisotropic noise maps and after that we apply the M82 mask or the U73 masks. Our results are shown in Table 2, where we emphasize that the χ^2 values were not divided by the number of d.o.f. The conclusion is that the Planck data, after being cut with either M82 or U73 masks, and independent of the addition of the inhomogeneous pixel's noise, are fully consistent with the Gaussian and statistically isotropy hypotheses of the standard cosmological model.

One should note that the overall good agreement – as evinced by the χ^2 test (table 2) – between the spectrum v_L^{PLA} and \bar{v}_L^G for the scale's range $L = 1, \dots, 10$, does not exclude the possibility that a particular scale L could be anomalous with respect to the Gaussian and statistically isotropic scenario. Indeed, one observes in Fig. 3, that the dipole v_1^{SMICA} is the largest multipole value of the spectra, being ~ 50 times greater than the sum of the other multipoles. This dominant dipole term, $L = 1$, similarly observed in the other three Planck maps, reflects what is being observed in the V^{PLA} -maps displayed in Fig. 2. Moreover, this dipolar variance asymmetry seems to be related to the anomalous variance distribution found in WMAP maps [84], and more recently in Planck data [10, 85]. For these reasons, this suspicious dipolar phenomenon deserves detailed angular scale's analyses, which shall be done in the next subsection.

To end this subsection, we notice that these results are robust under the four Planck's foreground-cleaning procedures, the set of Planck masks 2, inhomogeneous pixel's noise (released by Planck's team), and pixelization scheme parameters (that is, $N_{\text{side}} = 256; 512$, $N_{\text{hem}} = 768; 3,072$).

Planck map + mask	χ^2	$\chi^2_{inh.noise}$
SMICA + M82	8.6	8.2
SMICA + U73	8.8	8.6
NILC + M82	8.4	8.1
NILC + U73	9.0	8.7
SEVEM + M82	8.4	8.1
SEVEM + U73	8.6	8.3
CR + M82	11.6	11.1
CR + U73	12.9	12.4

Table 2. χ^2 , for 9 d.o.f., obtained when each \bar{v}_L^{PLA} spectrum is fitting the \bar{v}_L^{G} spectrum, considering the M82 and U73 masks, in two situations: ‘pure signal’ case and ‘signal + inhomogeneous noise’ case. The first (second) column correspond to the case without (with) the addition of inhomogeneous pixel’s noise to the Planck maps before the variance analysis. Our results show a good agreement between the large-angle spectra of V^{PLA} –maps as compared with V^{G} –maps. We stress that the V^{G} –maps are not normally distributed.

4.2 Angular-scale analyses of the Variance dipole

The observed direction of the dipolar variance maps, which appears close to the hemispherical NS-asymmetry [29, 40], brings the question about what are the CMB angular scales related to this phenomenon. Thus, we apply our variance estimator to the Planck and MC maps containing multipoles in a given range: $\ell \in [\ell_{\min}, \ell_{\max}]$, that is, only contributions in a such angular-scale interval. We consider the SMICA + VALmask case. The resulting confidence levels and variance dipole directions are summarized in the Table 3. Some of the V^{PLA} –maps corresponding to these angular-scales analyses are shown in Fig. 4. We found the following outcomes:

- For angular scales in the interval $\ell \in [2, 1,000]$, i.e. $\ell_{\max}=1,000$, we found that the statistical significance of the variance dipole has only 83.2 % CL, as compared to the dipoles from the V^{G} –maps, and points in the direction $(l, b) \simeq (245^\circ, -35^\circ)$. In other words, 168 dipole values, in the set of 1,000 $\{v_1^{\text{G}}\}$, have a larger value than v_1^{SMICA} .
- For the scales $\ell \in [2, 500]$ the variance dipole is, again, not statistically significant, 82.8 % CL; the direction being $(l, b) \simeq (245^\circ, -37^\circ)$.
- For $\ell \in [2, 40]$ we obtain a statistical confidence value of 71.0 % CL, with the dipole direction towards $(l, b) \simeq (250^\circ, -40^\circ)$.
- More interesting, for the CMB scales $\ell \in [41, 500]$ the phenomenon is more significant, 94.3 % CL, i.e., $\sim 2\sigma$, with direction towards $(l, b) \simeq (225^\circ, -15^\circ)$, close to the NS-asymmetry phenomenon direction.
- Remarkably, for the angular scales $\ell \in [4, 500]$ the variance dipole phenomenon is definitely statistically significant: 98.1 % CL, and the dipolar direction $(l, b) \simeq (220^\circ, -32^\circ)$ remains close to the NS-asymmetry phenomenon. Notice that removing the $\ell = 2, 3$ multipoles the significance increases, converting it in a statistically significant phenomenon: 82.8 % \rightarrow 98.1%, contrary to what was expected [84].

- Furthermore, for the case with only the quadrupole ($\ell = 2$) plus octopole ($\ell = 3$) CMB components, we found a low statistical significance: 14.0 % CL, with the dipole direction $(l, b) \simeq (310^\circ, -25^\circ)$. In addition, the analysis for the largest scales $\ell \in [2, 10]$ exhibits again a low significance: 44.3 % CL, with dipole direction $(l, b) \simeq (260^\circ, -47^\circ)$.

Contrary to the NS hemispherical asymmetry, where the signal comes from the low CMB multipoles (that is, large angular scales; see, e.g., [29], and references therein), our results show that the power of the variance dipole asymmetry phenomenon does not come only from the lowest multipoles ($\ell \leq 40$). Instead, we observe that the contribution from small scales $\ell \in [41, 500]$ is far from being negligible. The statistical evidence indicates that the contribution of the CMB multipoles $\ell \in [4, 500]$ to the variance dipole phenomenon is highly significant: $\sim 2.4\sigma$.

CMB angular-scales	CL (%)	(l, b)
$\ell \in [2, 1,000]$	83.2	$(245^\circ, -35^\circ)$
$\ell \in [2, 500]$	82.8	$(245^\circ, -37^\circ)$
$\ell \in [2, 40]$	71.0	$(250^\circ, -40^\circ)$
$\ell \in [41, 500]$	94.3	$(225^\circ, -15^\circ)$
$\ell \in [4, 40]$	92.2	$(220^\circ, -37^\circ)$
$\ell \in [4, 500]$	98.1	$(220^\circ, -32^\circ)$
$\ell \in [2, 10]$	44.3	$(260^\circ, -47^\circ)$
$\ell \in [2, 3]$	14.0	$(310^\circ, -25^\circ)$

Table 3. Statistical angular-scale analyses, showing the confidence level and the variance dipole direction for each interval investigated. Remarkably, for $\ell \in [4, 500]$ the variance dipole phenomenon is highly significant: $\sim 2.4\sigma$. Some of the V^{PLA} -maps corresponding to these angular-scales analyses are shown in Fig.4.

4.3 Masks and foreground residuals effects on Variance dipole

The four foreground-cleaned Planck maps, are expected to be free of contamination in the region outside their validation masks (i.e., outside the VALMASKS) [89]. Now we analyse the effect of the cut-sky masks on the variance dipole values obtained from different foreground-cleaned maps. In Fig. 5 it is shown that, for different values of f_{sky} , the mean variance dipole from simulations, \bar{v}_1^G , remains almost constant under the different cut-sky masks employed (see Table 1). However, this plot also exhibits that the values v_1^{PLA} decrease when larger masks are used. Two notable informations are concentrated in this interesting plot. The first one points against foreground residuals hypothesis: because all foreground-cleaned maps behaves identically when the same mask is used in their analysis, this is an strong indication that foregrounds residuals are absent in these maps. Second, from Fig. 5 there is a clear inference that the intensity of the dipole value from Planck maps is concentrated near the galactic plane, and for this reason much power is cut-off when larger masks are used.

We now investigate the frequency dependence of the V^{PLA} -maps, since it is well-known that galactic foregrounds depend on the electromagnetic frequency [89] and therefore their foreground residuals, if present, would manifest differently according to the individual frequency of the map in study. In accordance with this, and using the most severe cut-sky, i.e., the U73 mask, we produced the V^ν -maps for the individual frequency

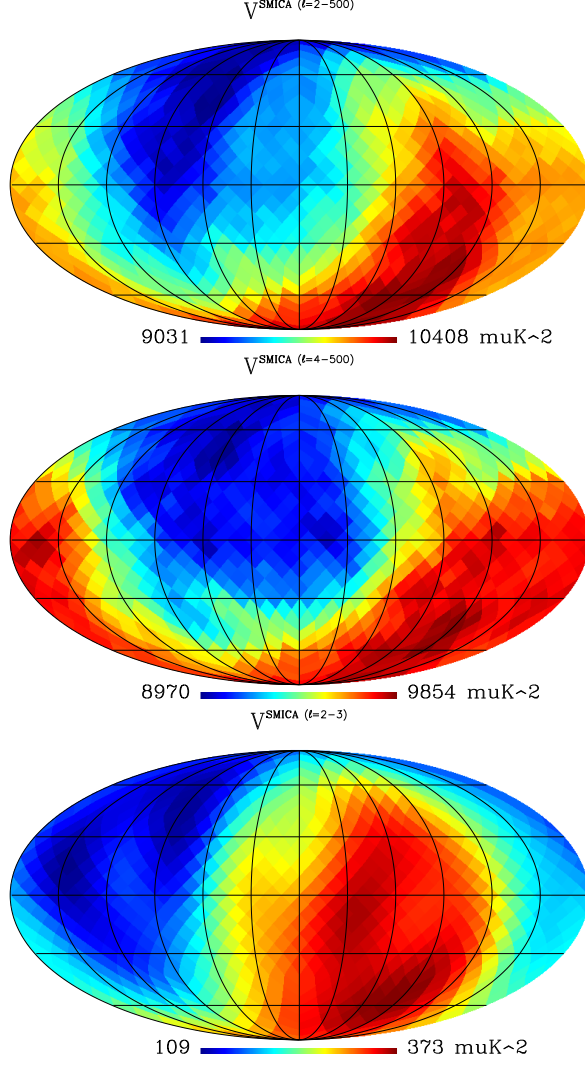


Figure 4. Variance dipole direction from the V^{SMICA} -map, obtained using its VALmask. In the upper panel we display the case $\ell \in [2, 500]$, in the middle panel the case $\ell = [4, 500]$, and in the bottom panel we show the $\ell \in [2, 3]$ case.

Planck maps of 70, 100, and 143 GHz. We found that their dipole values are quite similar: 2.44 , 2.33 , and $1.85 \times 10^5 \mu\text{K}^2$, respectively. Moreover, the dipole directions are also analogous: $(l, b) \simeq (245^\circ, -35^\circ)$, $(l, b) \simeq (240^\circ, -40^\circ)$, and $(l, b) \simeq (235^\circ, -35^\circ)$, respectively. Therefore, the fact that the variance dipoles v_1^ν for the individual frequency Planck maps, $\nu = 70, 100, 143$ GHz, are very similar, suggests that the galactic foreground residuals are not causing the variance dipole effect.

Our conclusion is, in accordance with [10] but in disagreement with a previous report [84], that galactic foregrounds are unlikely to be the cause of the variance dipole phenomenon. Although this conclusion is not new [10], its confirmation by a different statistical procedure is reassuring.

To end this subsection, we find interesting to explain why removing the quadrupole and the octopole components from data and simulations increases the statistical significance,

instead of decreasing it as claimed in [84]. The behavior of two quantities are relevant in this examination: the intensity, v_1^{PLA} , and the direction, (l, b) , of the variance dipole for the angular-scales in analyses. Regarding the role of the dipole direction: going from the case $\ell \in [2, 500]$ to the case $\ell \in [4, 500]$ the dipole direction changes from $(245^\circ, -37^\circ)$ to $(220^\circ, -32^\circ)$, that is, the net effect on the dipole direction after removing the $\ell = 2 - 3$ components is to point closer the galactic plane region (see Table 3). Regarding the intensity of the dipole: as commented above, from Fig. 5 one deduces that the strength of the dipoles v_1^{PLA} is concentrated near the galactic plane¹, and due to this fact much power is cut-off when larger masks are used. In this way, considering the galactic cuts, like $|b| \simeq 30^\circ$, used in [84] it is not difficult to understand that the dipole intensity is being cut-off in a larger fraction in the case $\ell \in [4, 500]$ as compared with the original case $\ell \in [2, 500]$. Differently from that galactic cuts, the VALmask used here is not so large near the region $(l, b) \sim (220^\circ, -32^\circ)$, so in our case the dipole intensity cut is moderate.

It is also worth to illustrate the role of the CMB multipole's intensity in the growth in the statistical confidence level when going from $\ell \in [2, 500]$ (82.8% CL) to the case $\ell \in [4, 500]$ (98.1% CL). The reason seems to be in the large difference between the low multipole's moments (in μK^2 units) $C_2 \simeq 250$ and $C_3 \simeq 480$ in Planck CMB maps, as compared with the corresponding values in Λ CDM and MCs spectra, namely, $C_2^{\Lambda\text{CDM}} = 1158$ and $C_3^{\Lambda\text{CDM}} = 545$ ². Because the quadrupole and octopole are notoriously lower for the Planck maps as compared with those of the MC produced from the Λ CDM spectrum, it makes intuitive sense that the variance dipoles from data and simulations are best compared in the range $\ell \in [4, 500]$ than in the interval $\ell \in [2, 500]$. To test this intuitive argument, we make the following experiment. Consider the SMICA map with its $\{a_{2m}\}$ and $\{a_{3m}\}$ components now multiplied by a numerical factor in such a way that its new quadrupole and octopole moments are $C_2^{\text{new}} = C_2^{\Lambda\text{CDM}}$ and $C_3^{\text{new}} = C_3^{\Lambda\text{CDM}}$. Then, we repeat the variance analysis for this map, considering the angular scales $\ell \in [2, 500]$, now finding that the statistical confidence level is 98.3 %, very similar with the 98.1 % CL found for the case $\ell \in [4, 500]$.

5 Concluding remarks

The Gaussian and statistically isotropic scenario, on which the Λ CDM concordance model is based, can be rigorously tested with precise CMB data from the four foreground-cleaned Planck maps. Although questions regarding the statistical homogeneity of the universe's large-scale structure wait for future large and deep surveys [94], other stimulating questions can be addressed with the highly precise CMB data from the Planck satellite.

Using a directional variance estimator, based on the *variance* statistical momentum, we performed a statistical analyses of the four foreground-cleaned Planck maps in several angular-scales intervals. In all the intervals investigated our results reveal a net dipolar distribution. In particular, in the angular scales $\ell \in [4, 40]$ and $\ell \in [41, 500]$ the significance is moderate, $\sim 2\sigma$. Moreover, for the multipoles range $\ell \in [4, 500]$, the result is highly significant $\sim 2.4\sigma$ (see Table 3), with the variance dipole pointing in the direction $(l, b) \simeq (220^\circ, -32^\circ)$, close to the direction of the NS-asymmetry phenomenon.

Additionally, we found that the Planck's variance dipole magnitude gets lower values for larger sky-cut masks, independent of the map analysed. This fact is coherent with the result that the variance dipole direction, for all the angular-scale intervals analysed, points

¹It was shown in [84] that the variance of the CMB data is not stable against the Galactic masks used.

²<http://pla.esac.esa.int/pla/aio/planckProducts.html>

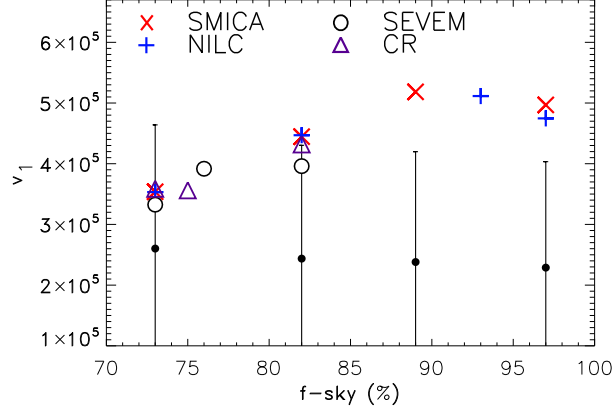


Figure 5. Plot of the v_1^{PLA} and \bar{v}_1^{G} values vs. the f_{sky} (see Table 1 for details). As observed, given a mask (i.e., f_{sky}), all the four foreground-cleaned Planck maps have almost equal v_1^{PLA} values. In other words, all Planck maps produce V^{PLA} -maps with the same dipole when the same mask is applied to them.

relatively near the galactic plane (see Table 3): in such a case, larger masks (i.e., lower f_{sky}) cut-off larger regions near this plane where most of the power is located.

Moreover, we found that foreground residuals are absent in our analyses because, considering the same mask, all the foreground-cleaned maps have essentially the same variance dipole value (with a slight dispersion of $\pm 3\%$, see Fig. 3). On the one other hand, this variance dipole stands robust in magnitude and direction against frequency dependence, in the 70, 100, and 143 GHz maps, disfavouring the foreground residuals cause, in agreement with [10].

Furthermore, an important part of the analyses of the foreground-cleaned Planck maps that validate our results was the robustness tests, where such examinations considered realistic features of the data like the inhomogeneous noise maps and galactic cut-sky masks (information released by the *Planck collaboration*³). The inhomogeneous noise comes out as a result of the non-uniform way the CMB sky is measured by the Planck probe. In fact, the regions near the ecliptic poles were observed by the probe many more times than others. The pixel's inhomogeneous noise data were released together with the foreground-cleaned Planck maps and are crucial to assert its influence in the hemispherical asymmetry found in the V^{PLA} -maps. In fact, although this noise has small magnitude, i.e. $|T| \lesssim 18 \mu\text{K}$ at 1σ level, the inhomogeneous noise has to be included in the analyses in order to quantify its impact in the results, and most importantly, to test the robustness of our outcomes. Our results show (see Table 2) that including pixel's inhomogeneous noise in the data analyses does not modifies appreciably our confidence level's calculation listed below. For instance, for the SMICA+VALMASK map, with and without noise, we obtain: $v_1^{\text{smica}+\text{noise}}/v_1^{\text{smica}} = 0.985$.

Summarizing, we conclude that our directional variance estimator shows a clear dipolar structure in the four foreground-cleaned and the individual frequency Planck maps, results that appear robust against the component separation algorithms, various Planck masks, map's pixelization parameters, and the addition of inhomogeneous pixel's noise. The mag-

³Based on observations obtained with Planck (<http://www.esa.int/Planck>), an ESA science mission with instruments and contributions directly funded by ESA Member States, NASA, and Canada.

nitude of this dipole is highly significant, $\sim 2.4\sigma$, in the angular scale interval $\ell \in [4, 500]$, attaining less significant values in the scales $\ell \in [4, 40]$ and $\ell \in [41, 500]$ (Table 3). We also discover that this significance is not so high in the range $\ell \in [2, 500]$ just because the C_2 and C_3 values in Planck CMB maps are manifestly lower than the corresponding values in the MC maps we use for analyses, which are based on Λ CDM spectrum. As a matter of fact, if we increase these multipoles values in Planck maps to be equal to those in MC data, we found that the statistical significance in this interval increases from 82.8% to 98.3%, i.e., 2.4σ .

Acknowledgments

TSP and AB acknowledge the support of Conselho Nacional de Desenvolvimento Científico e Tecnológico (CNPq) – Brasil. We acknowledge the use of the Planck data. Some of the results in this paper were derived using the HEALPix package [93].

References

- [1] **Planck Collaboration** Collaboration, P. Ade et al., *Planck 2013 results. I. Overview of products and scientific results*, [arXiv:1303.5062](#).
- [2] **Planck Collaboration** Collaboration, P. Ade et al., *Planck 2013 results. XV. CMB power spectra and likelihood*, [arXiv:1303.5075](#).
- [3] **Planck Collaboration** Collaboration, P. Ade et al., *Planck 2013 results. XVI. Cosmological parameters*, [arXiv:1303.5076](#).
- [4] **WMAP** Collaboration, C. Bennett et al., *Nine-Year Wilkinson Microwave Anisotropy Probe (WMAP) Observations: Final Maps and Results*, *Astrophys.J.Suppl.* **208** (2013) 20, [[arXiv:1212.5225](#)].
- [5] N. Bartolo, E. Komatsu, S. Matarrese, and A. Riotto, *Non-Gaussianity from inflation: Theory and observations*, *Phys.Rept.* **402** (2004) 103–266, [[astro-ph/0406398](#)].
- [6] E. Komatsu, N. Afshordi, N. Bartolo, D. Baumann, J. Bond, et al., *Non-Gaussianity as a Probe of the Physics of the Primordial Universe and the Astrophysics of the Low Redshift Universe*, [arXiv:0902.4759](#).
- [7] B. A. Bassett, S. Tsujikawa, and D. Wands, *Inflation dynamics and reheating*, *Rev.Mod.Phys.* **78** (2006) 537–589, [[astro-ph/0507632](#)].
- [8] A. D. Linde, *Inflationary Cosmology*, *Lect.Notes Phys.* **738** (2008) 1–54, [[arXiv:0705.0164](#)].
- [9] L. R. Abramo and T. S. Pereira, *Testing gaussianity, homogeneity and isotropy with the cosmic microwave background*, *Adv.Astron.* **2010** (2010) 378203, [[arXiv:1002.3173](#)].
- [10] **Planck Collaboration** Collaboration, P. Ade et al., *Planck 2013 results. XXIII. Isotropy and statistics of the CMB*, [arXiv:1303.5083](#).
- [11] L. R. Abramo, A. Bernui, I. S. Ferreira, T. Villela, and C. A. Wuensche, *Alignment Tests for low CMB multipoles*, *Phys.Rev.* **D74** (2006) 063506, [[astro-ph/0604346](#)].
- [12] L. R. Abramo, A. Bernui, and T. S. Pereira, *Searching for planar signatures in WMAP*, *JCAP* **0912** (2009) 013, [[arXiv:0909.5395](#)].
- [13] **Planck Collaboration** Collaboration, N. Aghanim et al., *Planck 2013 results. XXVII. Doppler boosting of the CMB: Eppur si muove*, [arXiv:1303.5087](#).

- [14] T. S. Pereira and L. R. Abramo, *Angular-planar CMB power spectrum*, *Phys.Rev.* **D80** (2009) 063525, [[arXiv:0907.2340](#)].
- [15] A. Bernui, T. Villela, C. A. Wuensche, R. Leonardi, and I. Ferreira, *On the cmb large-scales angular correlations*, *Astron.Astrophys.* **454** (2006) 409–414, [[astro-ph/0601593](#)].
- [16] A. Bernui, B. Mota, M. J. Reboucas, and R. Tavakol, *Mapping large-scale anisotropy in the wmap data*, *Astron.Astrophys.* **464** (2007) 479–485, [[astro-ph/0511666](#)].
- [17] A. Bernui, *Anomalous CMB north-south asymmetry*, *Phys.Rev.* **D78** (2008) 063531, [[arXiv:0809.0934](#)].
- [18] A. Bernui, *Is the cold spot responsible for the CMB North-South asymmetry?*, *Phys.Rev.* **D80** (2009) 123010, [[arXiv:0912.1147](#)].
- [19] P. Bielewicz, K. Górski, and A. Banday, *Low order multipole maps of CMB anisotropy derived from WMAP*, *Mon.Not.Roy.Astron.Soc.* **355** (2004) 1283, [[astro-ph/0405007](#)].
- [20] C. J. Copi, D. Huterer, and G. D. Starkman, *Multipole vectors - A New representation of the CMB sky and evidence for statistical anisotropy or non-Gaussianity at $2 \leq l \leq 8$* , *Phys.Rev.* **D70** (2004) 043515, [[astro-ph/0310511](#)].
- [21] D. J. Schwarz, G. D. Starkman, D. Huterer, and C. J. Copi, *Is the low- l microwave background cosmic?*, *Phys.Rev.Lett.* **93** (2004) 221301, [[astro-ph/0403353](#)].
- [22] C. J. Copi, D. Huterer, D. Schwarz, and G. Starkman, *On the large-angle anomalies of the microwave sky*, *Mon.Not.Roy.Astron.Soc.* **367** (2006) 79–102, [[astro-ph/0508047](#)].
- [23] C. Copi, D. Huterer, D. Schwarz, and G. Starkman, *The Uncorrelated Universe: Statistical Anisotropy and the Vanishing Angular Correlation Function in WMAP Years 1-3*, *Phys.Rev.* **D75** (2007) 023507, [[astro-ph/0605135](#)].
- [24] C. J. Copi, D. Huterer, D. J. Schwarz, and G. D. Starkman, *Large angle anomalies in the CMB*, *Adv.Astron.* **2010** (2010) 847541, [[arXiv:1004.5602](#)].
- [25] C. J. Copi, D. Huterer, D. J. Schwarz, and G. D. Starkman, *Lack of large-angle TT correlations persists in WMAP and Planck*, [[arXiv:1310.3831](#)].
- [26] C. J. Copi, D. Huterer, D. J. Schwarz, and G. D. Starkman, *Large-scale alignments from WMAP and Planck*, [[arXiv:1311.4562](#)].
- [27] M. Cruz, E. Martinez-Gonzalez, P. Vielva, and L. Cayon, *Detection of a non-gaussian spot in wmap*, *Mon.Not.Roy.Astron.Soc.* **356** (2005) 29–40, [[astro-ph/0405341](#)].
- [28] H. Eriksen, F. Hansen, A. Banday, K. Górski, and P. Lilje, *Asymmetries in the Cosmic Microwave Background anisotropy field*, *Astrophys.J.* **605** (2004) 14–20, [[astro-ph/0307507](#)].
- [29] H. K. Eriksen, A. Banday, K. Górski, F. Hansen, and P. Lilje, *Hemispherical power asymmetry in the three-year Wilkinson Microwave Anisotropy Probe sky maps*, *Astrophys.J.* **660** (2007) L81–L84, [[astro-ph/0701089](#)].
- [30] C. Gordon, W. Hu, D. Huterer, and T. M. Crawford, *Spontaneous isotropy breaking: a mechanism for cmb multipole alignments*, *Phys.Rev.* **D72** (2005) 103002, [[astro-ph/0509301](#)].
- [31] A. Gruppuso and K. M. Górski, *Large scale directional anomalies in the WMAP 5yr ILC map*, *JCAP* **1003** (2010) 019, [[arXiv:1002.3928](#)].
- [32] A. Gruppuso, F. Finelli, P. Natoli, F. Paci, P. Cabella, et al., *New constraints on Parity Symmetry from a re-analysis of the WMAP-7 low resolution power spectra*, *Mon.Not.Roy.Astron.Soc.* **411** (2011) 1445–1452, [[arXiv:1006.1979](#)].
- [33] N. Mandolesi, C. Burigana, A. Gruppuso, and P. Natoli, *Testing discrete symmetries with the cosmic microwave background: Current constraints and Planck forecasts*, *J.Phys.Conf.Ser.* **335** (2011) 012009.

- [34] F. K. Hansen, P. Cabella, D. Marinucci, and N. Vittorio, *Asymmetries in the local curvature of the WMAP data*, *Astrophys.J.* **607** (2004) L67–L70, [[astro-ph/0402396](#)].
- [35] F. K. Hansen, A. Banday, and K. Górski, *Testing the cosmological principle of isotropy: Local power spectrum estimates of the WMAP data*, *Mon.Not.Roy.Astron.Soc.* **354** (2004) 641–665, [[astro-ph/0404206](#)].
- [36] D. Huterer, *Mysteries on Universe’s Largest Observable Scales*, *New Astron.Rev.* **50** (2006) 868–874, [[astro-ph/0608318](#)].
- [37] T. Jaffe, A. Banday, H. Eriksen, K. Górski, and F. Hansen, *Evidence of vorticity and shear at large angular scales in the WMAP data: A Violation of cosmological isotropy?*, *Astrophys.J.* **629** (2005) L1–L4, [[astro-ph/0503213](#)].
- [38] T. Kahniashvili, G. Lavrelashvili, and B. Ratra, *CMB Temperature Anisotropy from Broken Spatial Isotropy due to an Homogeneous Cosmological Magnetic Field*, *Phys.Rev.* **D78** (2008) 063012, [[arXiv:0807.4239](#)].
- [39] T. Koivisto and D. F. Mota, *Anisotropic Dark Energy: Dynamics of Background and Perturbations*, *JCAP* **0806** (2008) 018, [[arXiv:0801.3676](#)].
- [40] K. Land and J. Magueijo, *The Axis of evil*, *Phys.Rev.Lett.* **95** (2005) 071301, [[astro-ph/0502237](#)].
- [41] K. Land and J. Magueijo, *The Axis of Evil revisited*, *Mon.Not.Roy.Astron.Soc.* **378** (2007) 153–158, [[astro-ph/0611518](#)].
- [42] A. de Oliveira-Costa, M. Tegmark, M. Zaldarriaga, and A. Hamilton, *The Significance of the largest scale CMB fluctuations in WMAP*, *Phys.Rev.* **D69** (2004) 063516, [[astro-ph/0307282](#)].
- [43] M. Tegmark, A. de Oliveira-Costa, and A. Hamilton, *A high resolution foreground cleaned CMB map from WMAP*, *Phys.Rev.* **D68** (2003) 123523, [[astro-ph/0302496](#)].
- [44] F. Paci, A. Gruppuso, F. Finelli, P. Cabella, A. De Rosa, et al., *Power Asymmetries in the Cosmic Microwave Background Temperature and Polarization patterns*, *Mon.Not.Roy.Astron.Soc.* **407** (2010) 399–404, [[arXiv:1002.4745](#)].
- [45] P. K. Rath and P. Jain, *Testing the Dipole Modulation Model in CMBR*, *JCAP* **1312** (2013) 014, [[arXiv:1308.0924](#)].
- [46] P. K. Samal, R. Saha, P. Jain, and J. P. Ralston, *Testing Isotropy of Cosmic Microwave Background Radiation*, *Mon.Not.Roy.Astron.Soc.* **385** (2008) 1718, [[arXiv:0708.2816](#)].
- [47] P. K. Samal, R. Saha, P. Jain, and J. P. Ralston, *Signals of Statistical Anisotropy in WMAP Foreground-Cleaned Maps*, *Mon.Not.Roy.Astron.Soc.* **396** (2009) 511, [[arXiv:0811.1639](#)].
- [48] P. Vielva, E. Martinez-Gonzalez, R. Barreiro, J. Sanz, and L. Cayon, *Detection of non-Gaussianity in the WMAP 1 - year data using spherical wavelets*, *Astrophys.J.* **609** (2004) 22–34, [[astro-ph/0310273](#)].
- [49] P. Vielva, Y. Wiaux, E. Martinez-Gonzalez, and P. Vanderghelynst, *Steerable wavelet analysis of CMB structures alignment*, *New Astron.Rev.* **50** (2006) 880–888, [[astro-ph/0609147](#)].
- [50] Y. Wiaux, P. Vielva, R. Barreiro, E. Martinez-Gonzalez, and P. Vanderghelynst, *Non-Gaussianity analysis on local morphological measures of WMAP data*, *Mon.Not.Roy.Astron.Soc.* (2007) [[arXiv:0706.2346](#)].
- [51] F. R. Urban and A. R. Zhitnitsky, *The Parity Odd Universe, Dark Energy and QCD*, *Phys.Rev.* **D83** (2011) 123532, [[arXiv:1011.2425](#)].
- [52] W. Zhao, *Directional dependence of CMB parity asymmetry*, *Phys.Rev.* **D89** (2014) 023010, [[arXiv:1306.0955](#)].
- [53] O. Fabre, S. Prunet, and J.-P. Uzan, *Topology beyond the horizon: how far can it be probed?*, [[arXiv:1311.3509](#)].

- [54] M. Hansen, J. Kim, A. Frejsel, S. Ramazanov, P. Naselsky, et al., *Can residuals of the Solar system foreground explain low multipole anomalies of the CMB ?*, *JCAP* **1210** (2012) 059, [[arXiv:1206.6981](#)].
- [55] D. Kashino, K. Ichiki, and T. T. Takeuchi, *Test for anisotropy in the mean of the CMB temperature fluctuation in spherical harmonic space*, *Phys.Rev.* **D85** (2012) 063001, [[arXiv:1112.0924](#)].
- [56] P. K. Rath, T. Mudholkar, P. Jain, P. K. Aluri, and S. Panda, *Direction dependence of the power spectrum and its effect on the Cosmic Microwave Background Radiation*, *JCAP* **1304** (2013) 007, [[arXiv:1302.2706](#)].
- [57] A. Rassat, J. L. Starck, P. Paykari, F. Sureau, and J. Bobin, *Planck CMB Anomalies: Astrophysical and Cosmological Foregrounds and the Curse of Masking*, [arXiv:1405.1844](#).
- [58] C. Bennett, R. Hill, G. Hinshaw, D. Larson, K. Smith, et al., *Seven-Year Wilkinson Microwave Anisotropy Probe (WMAP) Observations: Are There Cosmic Microwave Background Anomalies?*, *Astrophys.J.Suppl.* **192** (2011) 17, [[arXiv:1001.4758](#)].
- [59] **Planck Collaboration** Collaboration, P. Ade et al., *Planck 2013 results. XXII. Constraints on inflation*, [arXiv:1303.5082](#).
- [60] **Planck Collaboration** Collaboration, P. Ade et al., *Planck 2013 Results. XXIV. Constraints on primordial non-Gaussianity*, [arXiv:1303.5084](#).
- [61] E. Komatsu, *Hunting for Primordial Non-Gaussianity in the Cosmic Microwave Background*, *Class.Quant.Grav.* **27** (2010) 124010, [[arXiv:1003.6097](#)].
- [62] M. Liguori, E. Sefusatti, J. R. Fergusson, and E. Shellard, *Primordial non-Gaussianity and Bispectrum Measurements in the Cosmic Microwave Background and Large-Scale Structure*, *Adv.Astron.* **2010** (2010) 980523, [[arXiv:1001.4707](#)].
- [63] X. Chen, *Primordial Non-Gaussianities from Inflation Models*, *Adv.Astron.* **2010** (2010) 638979, [[arXiv:1002.1416](#)].
- [64] N. Jarosik, C. Bennett, J. Dunkley, B. Gold, M. Greason, et al., *Seven-Year Wilkinson Microwave Anisotropy Probe (WMAP) Observations: Sky Maps, Systematic Errors, and Basic Results*, *Astrophys.J.Suppl.* **192** (2011) 14, [[arXiv:1001.4744](#)].
- [65] M. Su, A. P. Yadav, M. Shimon, and B. G. Keating, *Impact of Instrumental Systematics on the CMB Bispectrum*, *Phys.Rev.* **D83** (2011) 103007, [[arXiv:1010.1957](#)].
- [66] E. Komatsu, *Wilkinson microwave anisotropy probe constraints on non-gaussianity*, *New Astronomy Reviews* **47** (2003), no. 8 797–803.
- [67] B. Gold, N. Odegard, J. Weiland, R. Hill, A. Kogut, et al., *Seven-Year Wilkinson Microwave Anisotropy Probe (WMAP) Observations: Galactic Foreground Emission*, *Astrophys.J.Suppl.* **192** (2011) 15, [[arXiv:1001.4555](#)].
- [68] D. Munshi, P. Valageas, A. Cooray, and A. Heavens, *Secondary non-Gaussianity and Cross-Correlation Analysis*, *Mon.Not.Roy.Astron.Soc.* **414** (2011) 3173, [[arXiv:0907.3229](#)].
- [69] N. Aghanim, S. Majumdar, and J. Silk, *Secondary anisotropies of the CMB*, *Rept.Prog.Phys.* **71** (2008) 066902, [[arXiv:0711.0518](#)].
- [70] C. P. Novaes and C. A. Wuensche, *Identification of galaxy clusters in cosmic microwave background maps using the Sunyaev-Zel'dovich effect*, *Astron.Astrophys.* **545** (2012) A34, [[arXiv:1211.5843](#)].
- [71] L.-Y. Chiang, P. D. Naselsky, O. V. Verkhodanov, and M. J. Way, *Non - gaussianity of the derived maps from the first-year WMAP data*, *Astrophys.J.* **590** (2003) L65–L68, [[astro-ph/0303643](#)].

- [72] P. D. Naselsky, O. V. Verkhodanov, L.-Y. Chiang, and I. D. Novikov, *Foreground analysis from the 1-year Wilkinson Microwave Anisotropy Probe (WMAP) data*, *Int.J.Mod.Phys.* **D14** (2005) 1273, [[astro-ph/0405523](#)].
- [73] J. Delabrouille, J.-F. Cardoso, M. L. Jeune, M. Betoule, G. Fay, et al., *A full sky, low foreground, high resolution CMB map from WMAP*, [arXiv:0807.0773](#).
- [74] C. Novaes, A. Bernui, I. Ferreira, and C. Wuensche, *Searching for primordial non-Gaussianity in Planck CMB maps using a combined estimator*, *JCAP* **1401** (2014) 018, [[arXiv:1312.3293](#)].
- [75] R. Saha, *A Foreground Cleaned CMB Map from Non-Gaussianity Measurement*, [arXiv:1105.6298](#).
- [76] D. Pietrobon, P. Cabella, A. Balbi, G. de Gasperis, and N. Vittorio, *Constraints on Primordial Non-Gaussianity from a Needlet Analysis of the WMAP-5 Data*, [arXiv:0812.2478](#).
- [77] D. Pietrobon, P. Cabella, A. Balbi, R. Crittenden, G. de Gasperis, et al., *Needlet Bispectrum Asymmetries in the WMAP 5-year Data*, [arXiv:0905.3702](#).
- [78] D. Pietrobon, A. Balbi, P. Cabella, and K. M. Górski, *Needatool: A Needlet Analysis Tool for Cosmological Data Processing*, *Astrophys.J.* **723** (2010) 1, [[arXiv:1010.1371](#)].
- [79] G. Pratten and D. Munshi, *Non-Gaussianity in Large Scale Structure and Minkowski Functionals*, *Mon.Not.Roy.Astron.Soc.* **423** (2012) 3209–3226, [[arXiv:1108.1985](#)].
- [80] T. L. Smith, M. Kamionkowski, and B. D. Wandelt, *The Probability Distribution for Non-Gaussianity Estimators*, *Phys.Rev.* **D84** (2011) 063013, [[arXiv:1104.0930](#)].
- [81] P. Vielva and J. Sanz, *Analysis of non-Gaussian CMB maps based on the N-pdf. Application to WMAP data*, [arXiv:0812.1756](#).
- [82] W. Zhao, *Probing the CMB cold spot through local Minkowski functionals*, *Res.Astron.Astrophys.* **14** (2014) 625–634, [[arXiv:1209.4021](#)].
- [83] C. Monteserin, R. B. Barreiro, P. Vielva, E. Martinez-Gonzalez, M. Hobson, et al., *A low CMB variance in the WMAP data*, *Mon.Not.Roy.Astron.Soc.* **387** (2008) 209–219, [[arXiv:0706.4289](#)].
- [84] M. Cruz, P. Vielva, E. Martinez-Gonzalez, and R. Barreiro, *Anomalous variance in the WMAP data and Galactic Foreground residuals*, [arXiv:1005.1264](#).
- [85] Y. Akrami, Y. Fantaye, A. Shafieloo, H. Eriksen, F. Hansen, et al., *Power asymmetry in WMAP and Planck temperature sky maps as measured by a local variance estimator*, *Astrophys.J.* **784** (2014) L42, [[arXiv:1402.0870](#)].
- [86] A. Bernui and M. Reboucas, *Searching for non-Gaussianity in the WMAP data*, *Phys.Rev.* **D79** (2009) 063528, [[arXiv:0806.3758](#)].
- [87] A. Bernui and M. Reboucas, *Non-gaussianity in the foreground-reduced CMB maps*, *Phys.Rev.* **D81** (2010) 063533, [[arXiv:0912.0269](#)].
- [88] A. Bernui and M. Reboucas, *Mapping the large-angle deviation from Gaussianity in simulated CMB maps*, *Phys.Rev.* **D85** (2012) 023522, [[arXiv:1109.6086](#)].
- [89] **Planck Collaboration** Collaboration, P. Ade et al., *Planck 2013 results. XII. Component separation*, [arXiv:1303.5072](#).
- [90] J.-F. Cardoso, M. Martin, J. Delabrouille, M. Betoule, and G. Patanchon, *Component separation with flexible models. Application to the separation of astrophysical emissions*, [arXiv:0803.1814](#).
- [91] R. Fernandez-Cobos, P. Vielva, R. Barreiro, and E. Martinez-Gonzalez, *Multi-resolution internal template cleaning: An application to the Wilkinson Microwave Anisotropy Probe 7-yr polarization data, 2012 MNRAS* **3** (420) 2162–2169, [[arXiv:1106.2016](#)].

- [92] H. K. Eriksen, C. Dickinson, C. Lawrence, C. Baccigalupi, A. Banday, et al., *CMB component separation by parameter estimation*, *Astrophys.J.* **641** (2006) 665–682, [[astro-ph/0508268](#)].
- [93] K. Górski, E. Hivon, A. Banday, B. Wandelt, F. Hansen, et al., *HEALPix - A Framework for high resolution discretization, and fast analysis of data distributed on the sphere*, *Astrophys.J.* **622** (2005) 759–771, [[astro-ph/0409513](#)].
- [94] **J-PAS Collaboration** Collaboration, N. Benitez et al., *J-PAS: The Javalambre-Physics of the Accelerated Universe Astrophysical Survey*, [arXiv:1403.5237](#).